

# A Model for Determining the Asperity Engagement Height in Relation to Web Traction Over Non-Vented Rollers

Brian S. Rice

Kevin A. Cole

Eastman Kodak Company,  
Rochester, NY 14652

Sinan Müftü<sup>1</sup>

Northeastern University,  
Department of Mechanical Engineering,  
Boston, MA 02115

*The traction developed between a thin flexible web, wrapped around a non-vented, rotating cylindrical roller is studied experimentally and theoretically. A series of eight webs representing a wide range of surface roughness characteristics are traction-tested against the same roller over a wide speed range. A mathematical model that couples air film pressure, web deflection, and asperity deformations is used to model the web/roller interface. An optimization technique is used to estimate the asperity compliance function parameters based on the experimental results and the mathematical model. A new model for determining the asperity engagement height, for surfaces with non-Gaussian peak height distribution, is proposed when the roughness of both surfaces is taken into account. Results are presented that indicate the viability and utility of the new methods.*

[DOI: 10.1115/1.1456087]

## 1 Introduction

Cylindrical rollers are used in supporting thin continuous materials known as webs in a wide range of web conveyance machinery (Fig. 1). In most applications, successful use of rollers is contingent on maintaining traction between the roller and web during transport. One effect, which can act to degrade traction performance, is air entrainment in the web/roller interface [1]. The converging geometry of the inlet region of the interface acts as a wedge bearing, resulting in superambient air pressure between the web and the roller. Thus, the web is partially supported by the air pressure, which results in reduction of the contact pressure between the web and the roller. This may eventually lead to relative motion (slip) between the web and the roller. Slip caused by traction loss can cause physical defects on the web such as scratches. In extreme cases, the web will completely lift off the roller surface, leading to a complete loss in traction between the web and the roller. Both of these are undesirable effects.

The tension, speed, and bending stiffness of the web, as well as the radius of the roller, air viscosity, and surface topographies of the web and the roller are the factors that have direct effects on the traction performance of webs over rollers. Traction is strongly influenced by the surface topography, with the smoother web/roller systems losing traction at lower web speeds than rougher systems. It is common to include additives onto the web to modify both the friction and roughness characteristics of the web and roller to help reduce traction loss sensitivity [2].

In general, surfaces of different kinds of webs can have very different peak-height distributions. For example, Figs. 2(b–d) give the WYKO images of three of the webs studied in this paper. Figure 2(b) (web-1) is a coated paper, and 2(c) (web-7) and 2(d) (web-8) are coated polyethylene terephthalate (PET) webs. The corresponding peak-height distributions are given in Fig. 3, which shows that the webs-1 and 8 are reasonably close to having a Gaussian distribution of the peak heights, whereas web-5 is not. Predictive models are required to consider these wide variations.

Knox and Sweeney [3] proposed a model using the foil bearing

equation [4], relating roller traction to off-line web-to-roller pressure/clearance measured at zero speed. Comparisons between predicted clearances and off-line measurements of surface topography showed that a few large asperities are more important for achieving high roller traction than a large number of small asperities. Ducotey and Good tested the traction characteristics of a single web over rollers with different surface roughnesses [5]. They found that traction can be maintained at higher speeds over rollers with rougher surfaces. Müftü and Altan provided a model, which considers the effects of asperity contact on the traction loss of a porous web moving over a stationary cylindrical guide [6]. They showed that, for a given web permeability, webs with smaller asperity engagement heights experience higher loss of contact pressure.

Contact occurs on the asperities that are inherently present on surfaces. The Greenwood and Williamson (GW) theory of contact pressure between two surfaces is based on the assumption that asperity-peaks make Hertzian contacts and that their distribution is Gaussian [7]. To predict contact pressure  $p_c$  as a function of the separation  $h$  for surfaces with a generic peak-height variation, an empirical model of the following form has been used [8–10]:

$$p_c = \beta \left( 1 - \frac{h}{\alpha_c} \right)^2 \quad \text{for } h \leq \alpha_c, \quad (1)$$

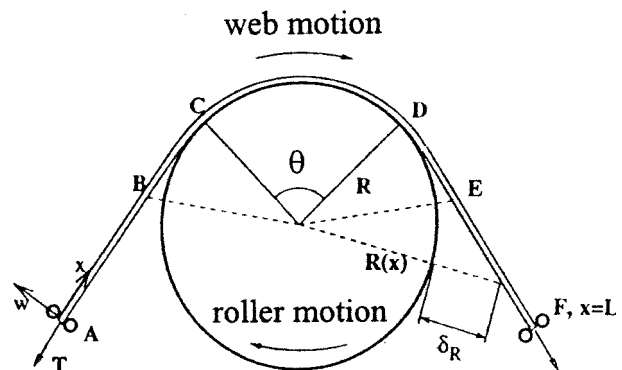
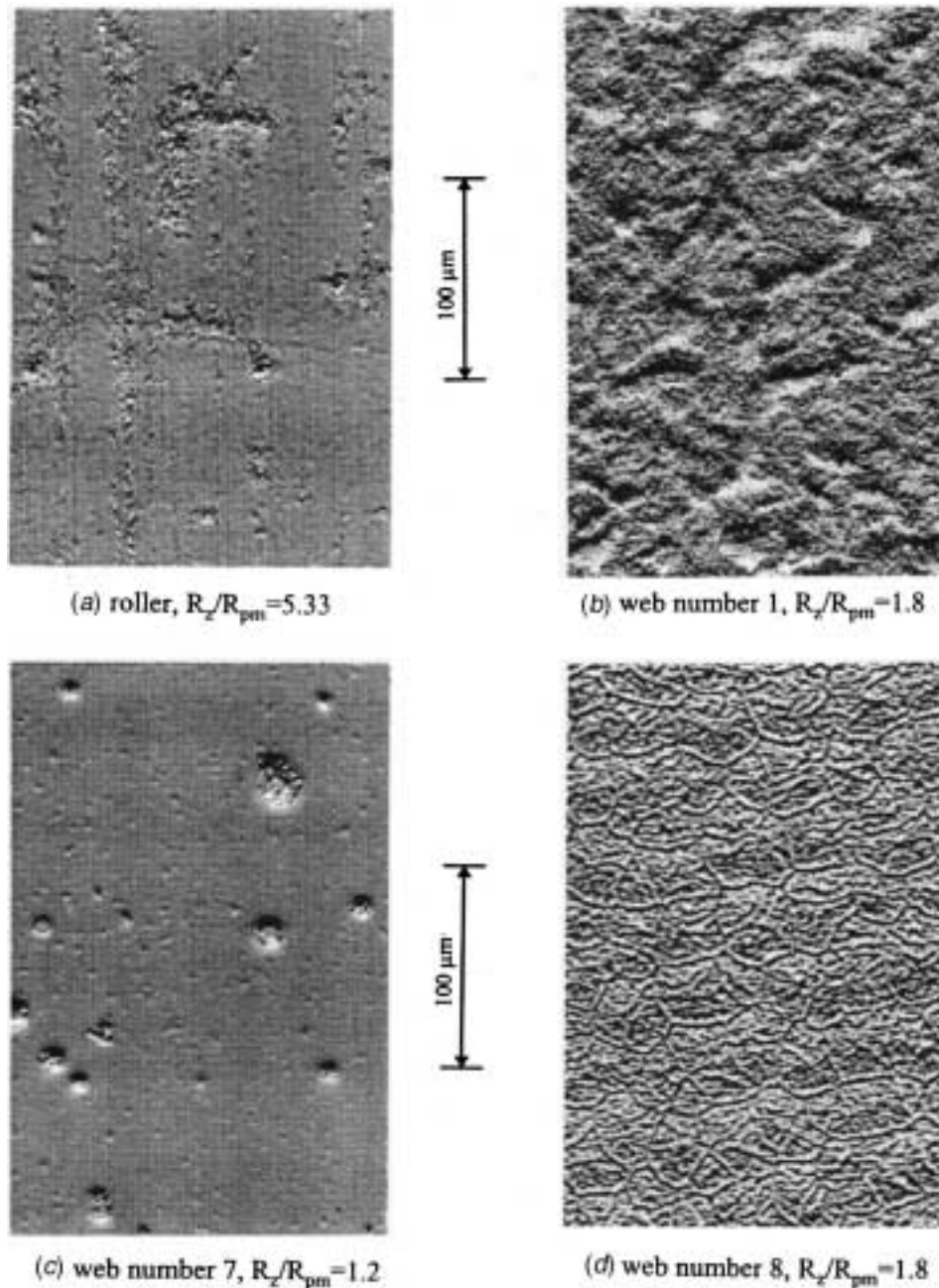


Fig. 1 Schematic view of a web conveyed over a cylindrical, rotating roller

<sup>1</sup>Most of this work has been done while the author was at M.I.T. Haystack Observatory.

Contributed by the Tribology Division for publication in the ASME JOURNAL OF TRIBOLOGY. Manuscript received by the Tribology Division February 9, 2001; revised manuscript received August 15, 2001. Associate Editor: C.-P. R. Ku.



**Fig. 2** Surface topography using non-contact interferometry at 250 $\times$  magnification: (a) roller,  $R_z/R_{pm}=5.33$ ; (b) web number 1,  $R_z/R_{pm}=1.8$ ; (c) web number 7,  $R_z/R_{pm}=1.2$ ; and (d) web number 8,  $R_z/R_{pm}=1.8$ .

where  $\beta$  and  $\alpha_c$  are the asperity compliance parameter and the composite asperity engagement height, respectively. The composite asperity engagement height is the maximum effective spacing between the web and roller just prior to complete loss of contact. The asperity compliance parameter is the pressure required to cause the web-to-roller spacing to go to zero. Typically these parameters are determined empirically from a load versus deflection curve using interferometry to measure the spacing between a web and a glass support structure [10].

The  $\alpha_c$  value is actually a combination of the surface asperity engagement height  $\alpha_s$  of each surface. For example, when a roller is in contact with a web  $\alpha_c$  is a combination of  $\alpha_r$  and  $\alpha_w$ , where  $r$  and  $w$  represent the roller and the web, respectively. This model is called the parabolic contact model. The goal of this paper is to

provide a simple experimental methodology to estimate the asperity compliance and the asperity engagement height for the parabolic contact model when the roughness of one or both surfaces is taken into account.

For this purpose, a series of eight webs representing a wide range of surface roughness characteristics are traction-tested against a rotating cylindrical roller over a wide speed range. A common way to measure and represent the traction characteristics of a web/roller interface is to introduce slip between the surfaces by applying a breaking torque on the roller [3,5]. In this case, the web tension will increase in the sliding direction and the exit tension  $T_e$  will be greater than the inlet tension  $T_i$ . As the slip occurs over the entire span of the wrap  $\theta$ , the well-known capstan formula applies,

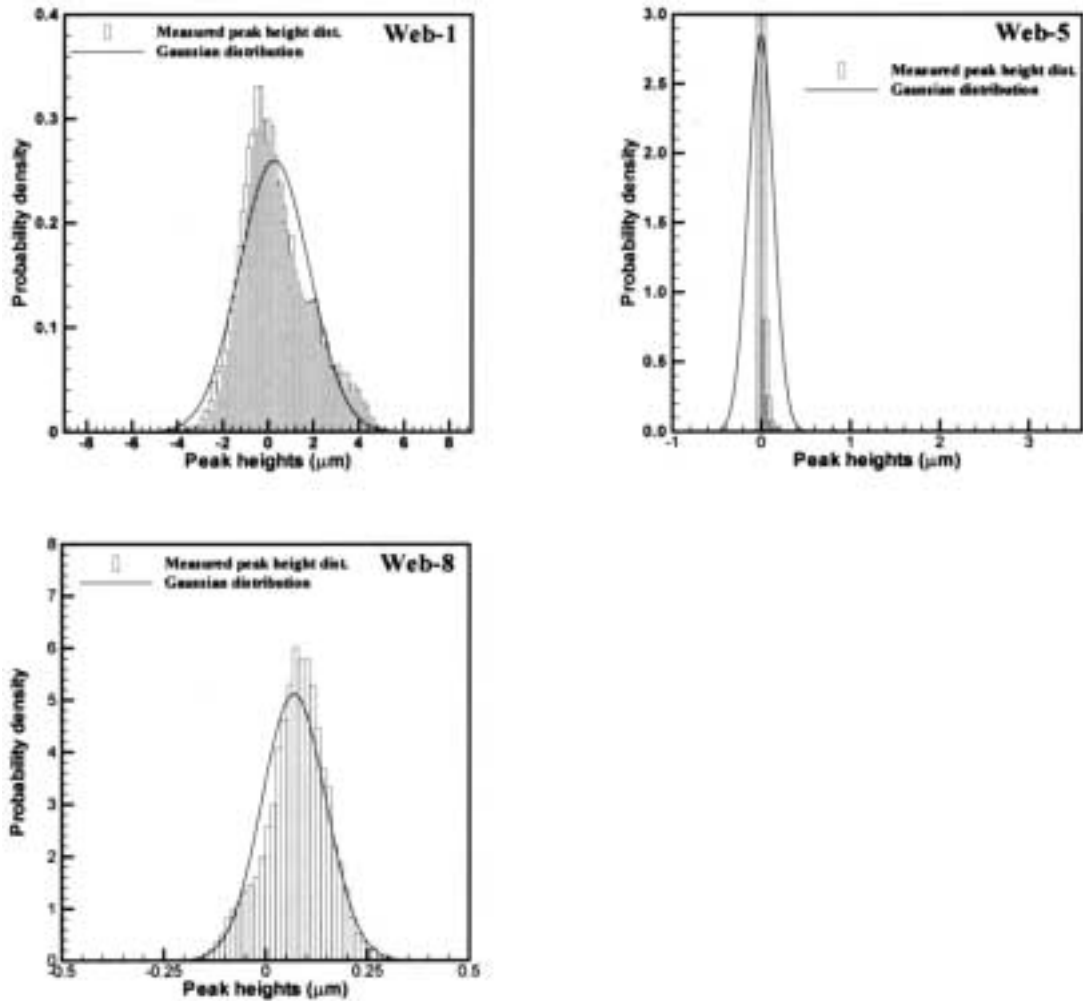


Fig. 3 Asperity peak height distribution for webs-1 and -5 and -8. Note that webs -5 and -7 have very similar surface topography characteristics. The Gaussian probability density distributions were calculated by using mean values of 0.35, 0, 0.08  $\mu\text{m}$  and standard deviations of 1.7, 0.19, 0.09  $\mu\text{m}$ , for webs-1, -5 and -8, respectively. The average skew values in these webs are 0.63, 13, 0.46, and the average Kurtosis values are 0.64, 220, 3.09, for webs-1, -5, and -8, respectively.

$$\mu = \frac{1}{\theta} \ln \left( \frac{T_e}{T_i} \right), \quad (2)$$

where  $\mu$  is the coefficient of friction between the roller and the web. For very slowly moving webs (e.g., 5 mm/s) the tension difference,  $\Delta T_o = T_{e_o} - T_{i_o}$ , is related by the low speed kinetic coefficient of friction,  $\mu_o$ . At increased web speeds the tension difference,  $\Delta T = T_e - T_i$ , decreases owing to partial air film support, and inlet and exit tensions are related by an equivalent high speed kinetic coefficient of friction,  $\mu_d$ . Note that in this representation,  $\mu_d \leq \mu_o$ .

A mathematical model of traction in the web/roller interface along with the empirical traction data is then used to generate optimal estimates of the contact model parameters. Web and roller surface roughness parameters are measured using an optical surface analyzer and web asperity compliance is measured using a stack compression test. These measured parameters are used to develop coefficients for the parabolic contact model and are compared to the optimized coefficients predicted by the mathematical traction model.

## 2 Mathematical Model of Traction in the Web/Roller Interface

Air lubrication in the web/roller interface is modeled using Reynolds equation, modified with a first-order slip-flow term [11]. For an infinitely wide compressible bearing, this equation becomes

$$\frac{\partial}{\partial x} \left[ p h^3 \frac{\partial p}{\partial x} \left( 1 + 6 \frac{\lambda_a}{h} \right) \right] = 6 \mu_a (V_w + V_r) \frac{\partial p h}{\partial x}, \quad (3)$$

where  $p$  is the air pressure in the clearance,  $\lambda_a$  is the molecular mean-free path of air,  $\mu_a$  is the air viscosity, and  $V_w$  and  $V_r$  are the web and roller velocities, respectively. The edges of the lubrication zone are located at points  $B$  and  $E$  as shown in Fig. 1. At these two points, the air pressure is set equal to the ambient pressure,  $P_{\text{atm}}$ .

The web deflections are modeled by using a modified form of the equation of equilibrium of an Euler-Bernoulli beam [6,12],

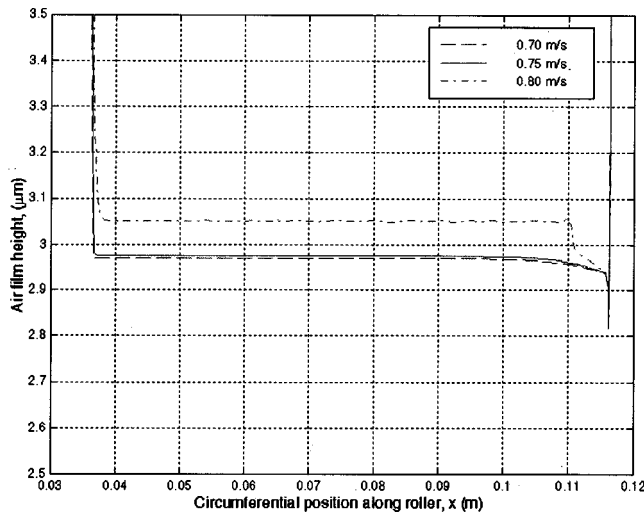


Fig. 4 The web-roller spacing at three different web speeds

$$D \frac{d^4(w-w_q)}{dx^4} + k(w-w_q) + (\rho V_w^2 - T) \frac{d^2(w-w_q)}{dx^2} = (p - P_{\text{atm}}) + p_c - \frac{T}{R(x)}, \quad (4)$$

where  $w$  is web deflection,  $w_q$  is the reference state of the web deflection, set when the web is quiescent ( $V_w = V_r = 0$ ) [6],  $x$  is the longitudinal spatial coordinate placed along the web,  $T$  is the web tension per unit width,  $\rho$  is the areal density of the web,  $P_{\text{atm}}$  is the ambient air pressure,  $D = Ec^3/12(1-\nu^2)$  is the bending stiffness, calculated by using the elastic modulus  $E$ , Poisson's ratio  $\nu$  and thickness  $c$  of the web. The web wraps the roller between the tangency points  $C$  and  $D$ . The web curvature,  $1/R(x)$ , causes the curved part of the web to gain an additional in-plane shell stiffness,  $k = Ec/R^2(x)(1-\nu^2)$ , and belt-wrap pressure,  $T/R(x)$ , acting radially inward. The curvature of the web is a continuous function of  $x$  [12]. The use of the quiescent reference state  $w_q$  is equivalent to allowing the web to settle on the asperity peaks without an attendant tension increase. Simple support conditions are assumed at the boundaries. The web-roller clearance is given by

$$h = w + \delta, \quad (5)$$

where  $\delta$  is a function representing the shape of the roller in the  $x$  coordinate [6]. The coupled systems of Eqs. (1), (2), (3), (4), and (5), are solved numerically using Newton's method [6,13].

A typical result from the coupled model is shown in Fig. 4.

Here, the web roller clearance  $h$  is plotted against roller circumferential position for  $V_w = V_r = 0.7, 0.75,$  and  $0.8$  m/s respectively. The other parameters of the problem are as follows:  $R = 5.08$  cm,  $\theta = 90$  deg,  $c = 10$   $\mu\text{m}$ ,  $\rho = 0$ ,  $T = 175$  N/m,  $\mu_a = 1.85 \times 10^{-5}$  Pa·s,  $\lambda_a = 63$  nm,  $\alpha_c = 3$   $\mu\text{m}$  and  $\beta = 10$  MPa. The grid spacing used in all of the simulations is  $50$   $\mu\text{m}$ .

The result shows that web deflection increases with speed. The web is fully in contact with the roller at  $0.7$  and  $0.75$  m/s, where the asperities are compressed to  $2.98$   $\mu\text{m}$ . The web begins to be fully supported by air when  $0.75 \leq V_w \leq 0.8$  m/s. This agrees very favorably with the predictions using the foil bearing equation,  $h = 0.643R(6\mu_a(V_w + V_r)/T)^{2/3}$  [4], which yields a web speed of  $0.74$  m/s for a clearance of  $3$   $\mu\text{m}$ . The results also indicate that the trailing edge flies at a lower clearance relative to the entry and mid-wrap regions because of the negative air pressure (not shown) that characteristically develops at the exit side of a foil bearing [14]. This behavior will have the effect of delaying complete web-to-roller traction loss to higher speeds than would be predicted using the simple foil bearing.

In this work, a macroscopic approach is taken to evaluate the equivalent coefficient of friction using the model. This approach makes the assumption that the equivalent coefficient of friction  $\mu_m$  is linearly related to the contact force  $F_c$  and low speed kinetic coefficient of friction  $\mu_o$  and is inversely related to the belt wrap force,  $F_b$ , as,

$$\mu_m = \mu_o \frac{F_c}{F_b}, \quad (6)$$

where  $F_c = \int_0^L p_c dx$  and  $F_b = \int_0^L T/R(x) dx$ . Note since the model does not include the effect of tension changes around the wrap, the average of inlet and exit tensions,  $T_a = (T_e + T_i)/2$ , is used in Eq. (4).

### 3 Experimental Measurements and Results

A series of eight webs were traction-tested experimentally: one polyethylene coated paper, one cellulose triacetate (CTA), and five polyethylene terephthalate (PET) films. The PET webs had a wide range of coatings, which caused significant surface roughness differences between them. A description of each web is provided in Table 1. A non-vented anodized aluminum roller with a radius of  $5.08$  cm and width of  $1.5$  m was used in all the tests. The following measurements were made to provide data to develop and validate the surface roughness contact model:

- narrow-width low-speed kinetic coefficient of friction between the roller and webs,
- full-width high-speed equivalent coefficient of friction between the roller and webs,
- surface roughness of the webs and roller,
- stack compression measurements for three of the eight webs.

Table 1 Web description

web #	description	thickness ( $\mu\text{m}$ )	width (m)	density ( $\text{kg/m}^3$ )	Elastic Modulus (GPa)
1	Polyethylene coated paper	272	0.75	1108	4.14
2	coated Polyethylene Terephthalate	182	0.75	1358	4.83
3	coated Polyethylene Terephthalate	179	0.75	1358	4.83
4	uncoated Polyethylene Terephthalate	98	0.75	1358	4.83
5	coated Polyethylene Terephthalate	183	0.75	1358	4.83
6	coated Cellulose Triacetate	122	0.75	1358	4.14
7	coated Polyethylene Terephthalate	176	0.75	1358	4.83
8	coated Polyethylene Terephthalate	118	0.75	1358	4.83

Table 2 Coefficient of friction experimental data

Dynamic traction test conditions:								
0.102 m dia. roller with 90 degree wrap								
0.75 m wide web at 175N/m unit tension								
speed (m/s)	web 1	web 2	web 3	web 4	web 5	web 6	web 7	web 8
0.005 <sup>a</sup>	0.21	0.16	0.18	0.21	0.18	0.19	0.19	0.20
0.13		0.20	0.20	0.20				0.15
0.15			0.18	0.18				0.11
0.23			0.16	0.16				
0.25	0.33	0.18						
0.28					0.13	0.13	0.13	0.05
0.51	0.30	0.15	0.08	0.08	0.07	0.07	0.07	0.00
1.02		0.10	0.01	0.01	0.01	0.01	0.01	
1.52		0.07						
2.03		0.04						
2.54	0.09	0.03						
5.08	0.04							
7.62	0.01							

a. All 0.005m/s speed traction coefficients are from ASTM G143 test. The 95% confidence limits on the mean for the ASTM G143 tester are +/- 0.01. All other traction coefficients are from the dynamic traction test. The 95% confidence limits on the mean for the dynamic traction test are +/- 0.01.

The results of these measurements are discussed in sections 3.1–3.4.

**3.1 Low-Speed Kinetic Coefficient of Friction—Narrow-Width.** The kinetic coefficient of friction of the web-to-roller system was measured for all eight webs using a standard ASTM (G143-96) test method [15]. Three 25 mm wide strips were removed from different widthwise locations of each web. Each strip was tested under following conditions: 90 degrees of wrap, 87.5 N/m low side tension and a slip speed of 5 mm/s with the roller held stationary. The measurements were made at 70°F and 40 percent relative humidity. The average low speed kinetic coefficient of friction  $\mu_o$  for each web is shown in the first row of Table 2. The 95 percent confidence limits are  $\pm 0.01$ .

**3.2 High-Speed Equivalent Coefficient of Friction—Full-Width.** The equivalent coefficient of friction between each of the webs and the roller were measured at speeds ranging from 0.13 to 7.62 m/s. Figure 5 schematically depicts the dynamic traction tester used to measure the full-width, high-speed, equivalent coefficient of friction  $\mu_d$ . This device operates in an endless band mode. The lowest speed at which the dynamic traction tester can be used reliably is 0.13 m/s. For several webs the lowest test speed was 0.25 m/s or greater. All the webs were tested at 70°F and 50 percent relative humidity and were 0.75 m wide by 30 m long.

In order to measure the high-speed, equivalent coefficient of friction  $\mu_d$ , slip was induced between the web and the roller, by applying a braking torque to the roller, until a 0.03 percent speed

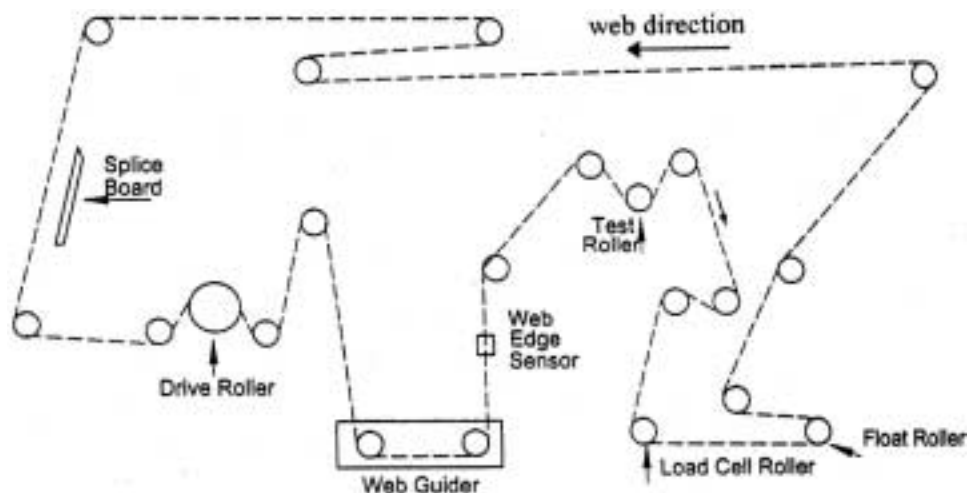


Fig. 5 Schematic of the dynamic traction tester

Table 3 Surface roughness data

	$R_{pm}$			$R_z$		
	mean	std	+/-95% c.i.	mean	std	+/-95% c.i.
roller	1.44	0.12	n/a	7.67	2.09	n/a
web 1	6.08	0.62	0.99	10.88	0.60	0.96
web 2	4.99	0.62	0.98	5.74	0.66	1.05
web 3	1.04	0.14	0.22	1.22	0.20	0.32
web 4	0.61	0.30	0.48	0.72	0.32	0.51
web 5	2.07	0.18	0.28	2.98	0.10	0.16
web 6	0.80	0.08	0.13	0.99	0.14	0.22
web 7	1.03	0.18	0.29	1.24	0.23	0.36
web 8	0.68	0.06	0.10	1.20	0.10	0.16

Number of samples equals 4 for webs and 2 for roller. All units are in  $\mu\text{m}$ .

difference between the roller and the web took place. Each measurement was repeated three times. The value of  $\mu_d$  was computed from the average of the three torque values using Eq. (2). Based on the location of the tension setting device (float roller), the exit tension was fixed at 175 N/m and the inlet tension dropped in proportion to the applied torque to the roller.

The  $\mu_d$  values for webs-1 through 3 at 0.25 and 0.13 m/s are higher than  $\mu_o$  values based on the 95 percent confidence limits. For web-1, the values of friction at 0.005 and 0.25 m/s were so widely different that the 0.33 value was used for  $\mu_o$ . For the other seven webs, the equivalent coefficient of friction from the ASTM G143 tester was used for  $\mu_o$ . Some possible explanations for these differences are: (a) widthwise variations in low speed kinetic coefficient of friction; (b) relative humidity differences between the two tests, and (c) variations in average tension between the two tests. The effects of  $\mu_o$  errors are discussed in detail in section 4.1.1.

**3.3 Web/Roller Surface Roughness.** Web and roller surface roughness was measured using a commercially available optical surface profiler (WYKO). Sample size was  $460 \mu\text{m} \times 600 \mu\text{m}$  with an 820 nm resolution. For each web, four locations across the width were measured. At each of the four locations five measurements were made within 10 mm of each other. Table 3 shows the overall average, standard deviation, and 95 percent confidence limits for all eight webs. Two roughness parameter measures are reported: the average of the five highest peaks in the sample with respect to the mean plane,  $R_{pm}$ , and the difference between the average of the five highest peaks and five lowest valleys in the sample measured from the mean plane,  $R_z$ . For the roller, two locations were measured: one near the roller center and the other 0.375 m from the center of the roller. Again at each location five measurements were made within 10 mm of each other. Table 3 shows the overall average and standard deviation for the roller.

**3.4 Stack Compression Measurements.** This test consists of measuring the load/displacement behavior of three different 5.1 mm high stacks of individual plies (each ply measures 12.7 mm  $\times$  50.8 mm) cut from the web. This test was done for webs-1, 5, and 8. The displacements were measured relative to zero pressure, and the results were averaged after being normalized to a per ply basis. This data is used to estimate the parameter  $\beta$  by regression analysis. Values of  $\beta$  for webs-1, 5, and 8 were found to be 20,850 Pa, 12,500 Pa, and 88,800 Pa, respectively. This method assumes that both front and back surfaces have equal stiffness and the roller surface roughness has no influence on compliance. Both assumptions can lead to obvious errors, but as will be shown in the next section,  $\beta$  has only a secondary effect on traction.

#### 4 Determination of the Contact Parameters

The empirical parabolic contact pressure model given in Eq. (1) involves two parameters  $\alpha_c$  and  $\beta$ . In this section the following are discussed:

- a method for determining these two parameters, based on minimizing the equivalent coefficient of friction error between the experiments and the model,
- description of a new model to define  $\alpha_s$ , based on easily measurable surface topography parameters, and
- a heuristic formula for calculating the composite engagement height  $\alpha_c$  of two rough surfaces in contact.

**4.1 Determination of Contact Parameters Based on Traction Experiments and Model.** If it is assumed that the surface asperities deform according to the parabolic model given by Eq. (1), then it is possible to determine  $\alpha_c$  and  $\beta$  from the experimentally measured coefficient of friction values,  $\mu_d$ . This can be achieved by minimizing the squared-error  $\varepsilon^2$  between the experimental,  $\mu_d$ , and predicted,  $\mu_m$ , coefficient of friction values, over the tested web speeds, by varying  $\alpha_c$  and  $\beta$ . The squared-error is defined as,

$$\varepsilon^2 = \sum_{i=1}^{i \max} (\mu_{di} - \mu_{mi})^2, \quad (7)$$

where the index  $i$  ranges over the speeds of interest and  $i \max$  is the total number of test points. The error-minimization requires the simultaneous solution of Eqs. (1) and (3–6) for a wide range of the parameters  $\alpha_c$  and  $\beta$ . The error-gradient information during this search suffers from numerical noise of this solution, thus standard optimization procedures which require gradient information experience difficulty in finding the global minimum. Therefore, a *grid-search method* consisting of two sweeps is used. In the first sweep, a  $10 \times 10$  grid of  $\alpha_c$  and  $\beta$  values, covering a wide range of these parameters, are tested for each speed (i.e., each  $i$  in Eq. (7)). This gives the first-optimal ( ${}^m\alpha_c, {}^m\beta$ ) pair. Then, the ranges of  $\alpha_c$  and  $\beta$  are refined around this solution by again choosing ten values for each one of the variables. The result of the second sweep is declared the optimal pair ( ${}^m\alpha_c, {}^m\beta$ ) that minimizes  $\varepsilon^2$ . These optimal values are tabulated in columns two and three of Table 4.

**4.1.1 Effect of  $\mu_o$  on the Optimal Values of Contact Parameters.** Considering the uncertainty in the experimental value of  $\mu_o$ , it was decided that an investigation of the effect of this parameter on the optimal value for the composite asperity engagement height,  ${}^m\alpha_c$ , and the optimal value for asperity compliance,  ${}^m\beta$ , was warranted. Consider web-5, for which  $\mu_o=0.18$  (Table

Table 4 Optimized engagement height and compliance

	${}^m\alpha_c$	${}^m\beta$	${}^m\alpha_c$ range	${}^m\beta$ range	$\mu_o$ range
web 1	9.5	20	8.0 - 10.0	40 - 5	0.30 - 0.45
web 2	7.5	27.5	7.0 - 9.0	45 - 5	0.15 - 0.30
web 3	4.0	40	4.0 - 4.5	45 - 5	0.15 - 0.30
web 4	3.7	37.5	4.0 - 4.5	45 - 5	0.15 - 0.30
web 5	4.0	22.5	4.0 - 4.0	45 - 5	0.15 - 0.30
web 6	4.0	17.5	4.0 - 4.0	45 - 5	0.15 - 0.30
web 7	4.0	17.5	4.0 - 4.0	45 - 5	0.15 - 0.30
web 8	2.0	40	2.0 - 2.5	40 - 10	0.15 - 0.30

$\alpha$  is in  $\mu\text{m}$  and  $\beta$  is in kPa

2). The effect of  $\mu_o$  values of 0.15, 0.2, 0.25, and 0.3 on finding the optimal ( ${}^m\alpha_c, {}^m\beta$ ) was tested within  $1 \leq {}^m\alpha_c \leq 10 \mu\text{m}$  and  $5 \leq {}^m\beta \leq 45 \text{ kPa}$  ranges. Figure 6 gives the contours of  $\varepsilon^2$  for these four  $\mu_o$  values. The optimal values are indicated on the plots. This figure shows that, as the error is reduced, the contours of  $\varepsilon^2$  become essentially parallel to the  ${}^m\beta$  axis. For the four different  $\mu_o$  values listed above, the optimal values of  ${}^m\beta$  are 45, 15, 10, and 5 kPa, respectively, while the optimal  ${}^m\alpha_c$  value remains at 4  $\mu\text{m}$ .

Similar tests were repeated for all of the webs and it was found that this characteristic is typical for all. The results of these tests for all eight web/roller combinations are summarized in Table 4. This table, like Fig. 6, shows that the steady state equilibrium in the web-roller interface is influenced more significantly by the engagement height  $\alpha_c$ , than by the compliance  $\beta$  or the coefficient of friction  $\mu_o$ . This can be explained by looking at  $\mu_d$ -versus-speed curves for  $\beta=22.5$  and 225 kPa as shown in Fig. 7. In the low- $\beta$  case the asperities are expected to deflect more

than in the high- $\beta$  case, when the same contact pressure is applied. More asperity deflection results in a lower web-roller clearance, which in turn causes higher air pressure build-up in the interface. Therefore, the webs with more compliant asperities lose more traction at a given web speed than the webs with stiffer asperities. However, as shown in Fig. 7, a factor of ten difference in  $\beta$  causes a relatively small change in the  $\mu_d$ -versus-speed behavior. Hence, it can be concluded that  $\beta$  has a small influence on the  $\mu_d$  variation.

#### 4.2 Engagement Height Based on Surface Topography.

The error minimization analysis already gives composite surface roughness  $\alpha_c$  to be used in Eq. (1), based on the results of the traction experiments. The goal in this section is to introduce a measure of the engagement height, based on the easily measurable surface parameters  $R_{pm}$  and  $R_z$ , that gives good correlation with  $\alpha_c$ . This is achieved in two steps: first, a model is proposed to

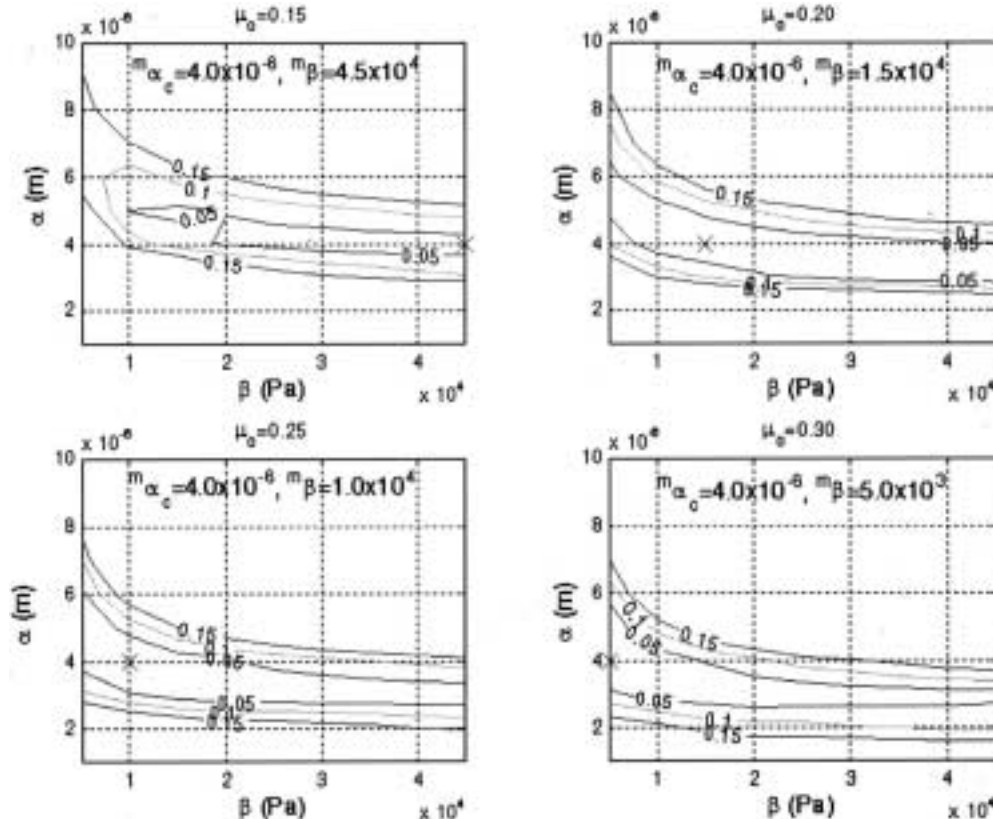


Fig. 6 Optimization contours for web-5 for various  $\mu_o$ . Optimum locations are indicated by X.

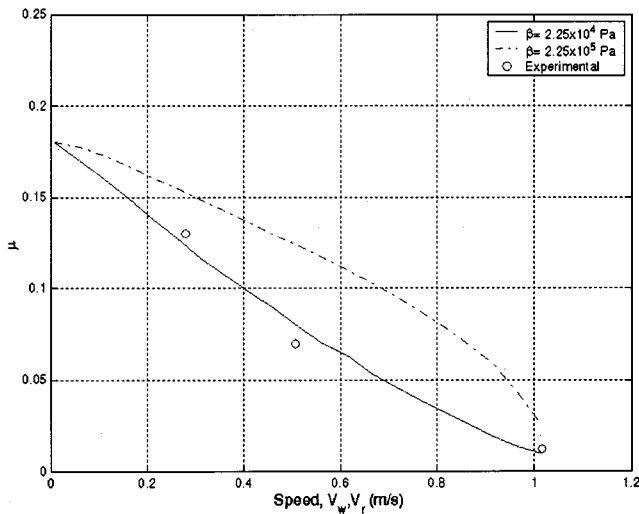


Fig. 7 Predicted traction curves for  $\beta=22.5$  kPa and  $\beta=225$  kPa and the measured traction values

calculate  $\alpha_s$  of an individual surface based on the topography of the surface; then, a method is described for calculating  $\alpha_c$  of two surfaces in contact.

**4.2.1 Model for Engagement Height  $\alpha_s$  Based on Surface Topography.** Wu and Talke showed that a peak-to-valley surface roughness  $R_z$  worked well to predict the asperity engagement height  $\alpha_c$ , when a relatively rough tape comes in contact with a smooth glass surface [10]. While this appears to be true for magnetic tapes whose asperity heights have a Gaussian distribution, the authors find that, in general, using  $R_z$  alone can be misleading.

In order to illustrate this point, Fig. 8 depicts 3 different surfaces: a surface with a few peaks (case-1), a surface with a few valleys (case-2) and a surface with equal number of peaks and valleys (case-3). These surface topographies are non-Gaussian, but they are encountered in many web handling applications. When a smooth web comes in contact with the rollers, e.g., case-1 and case-2, it can be seen that the true engagement height is significantly larger for case-1, even though  $R_z$  is the same for both roller surfaces. Case-3 has a  $R_z$  value twice as large as cases-1 and -2. The engagement height for case-3 is larger than that of case-1

but probably not twice as large, as  $R_z$  alone would suggest. This shows that for non-Gaussian surfaces  $R_z$  alone is not a good measure of the asperity engagement height  $\alpha_s$ .

The  $R_z/R_{pm}$  ratio for the roller in cases-1, 2, and 3 given in Fig. 8 are approximately 1, much greater than 1 and approximately 2, respectively. Thus, in this context, the  $R_z/R_{pm}$  ratio describes a rough surface as follows:

- $R_z/R_{pm} \cong 1$ : only a few peaks and even fewer valleys
- $R_z/R_{pm} \gg 1$ : only a few valleys and even fewer peaks
- $R_z/R_{pm} \cong 2$ : an equal number of peaks and valleys of nearly same amplitude.

It seems that a measure for  $\alpha_s$  that combines  $R_z$ ,  $R_{pm}$  and  $R_z/R_{pm}$  would be appropriate in order to capture these effects. To this end, the following heuristic model is proposed for estimating  $\alpha_s$  when a smooth surface comes into contact

$$\alpha_s = R_{pm} + \frac{(R_z - R_{pm})}{(R_z/R_{pm})} \quad (8)$$

In this relation,  $\alpha_s$  approaches  $R_{pm}$  as  $R_z/R_{pm} \cong 1$ ,  $0.5(R_z + R_{pm})$  as  $R_z/R_{pm} \cong 2$ , and  $2R_{pm}$  as  $R_z/R_{pm} \gg 1$ . Thus, it is seen that the engagement height lies in the range  $R_{pm} \leq \alpha_s \leq 2R_{pm}$ .

It is reasonable to assume that the surfaces with Gaussian distribution of asperity peaks would have  $R_z/R_{pm} \cong 2$ . Therefore the engagement height  $\alpha_s = 0.5(R_z + R_{pm})$ , predicted by using Eq. (8), is only slightly lower than the measurements in [10].

**4.2.2 The Composite Engagement Height  $\alpha_c$  of Two Surfaces in Contact.** For the eight web/roller combinations studied in this paper, the roughness of both surfaces is significant. Therefore, the composite engagement height,  $\alpha_c$ , should represent the roughness of both surfaces. For Gaussian surfaces,  $\alpha_c$  can be obtained by the root-mean-square (rms) of the engagement heights of the two surfaces [16]. This may not be applicable in general. For example, consider the three idealized surfaces presented in Fig. 9. In case-1, the roller has a surface comprised of high-frequency roughness with equal peaks and valleys, while the web has a few peaks; in case-2, both the web and the roller have high-frequency roughness with equal peaks and valleys; and in case-3, the web and roller have a few peaks and valleys. For calculating  $\alpha_c$  of these surfaces, a *sum-model*, a *rms-model*, and a *max-model* are proposed for case-1, case-2, and case-3, respectively.

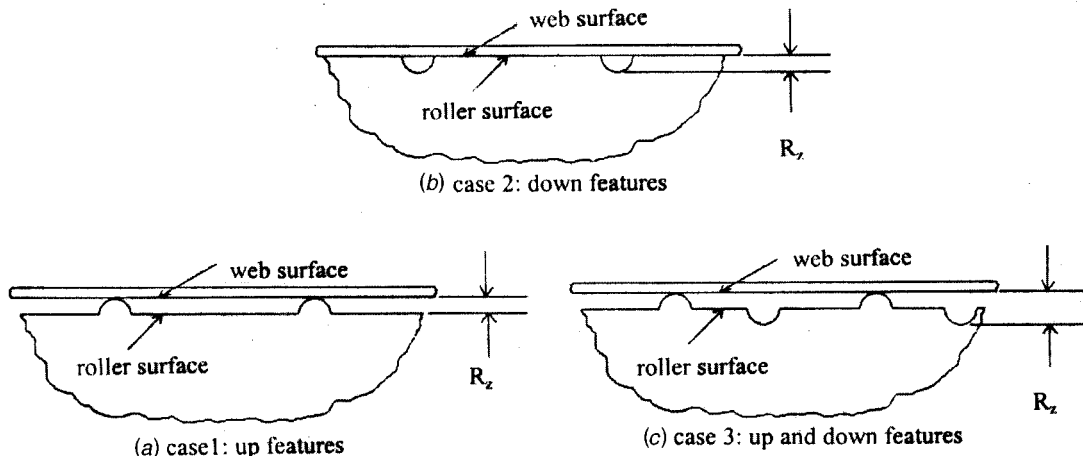


Fig. 8 Pictorial representation of contact between a smooth web and various idealized roller surface textures: (a) case 1: up features; (b) case 2: down features; and (c) case 3: up and down features.

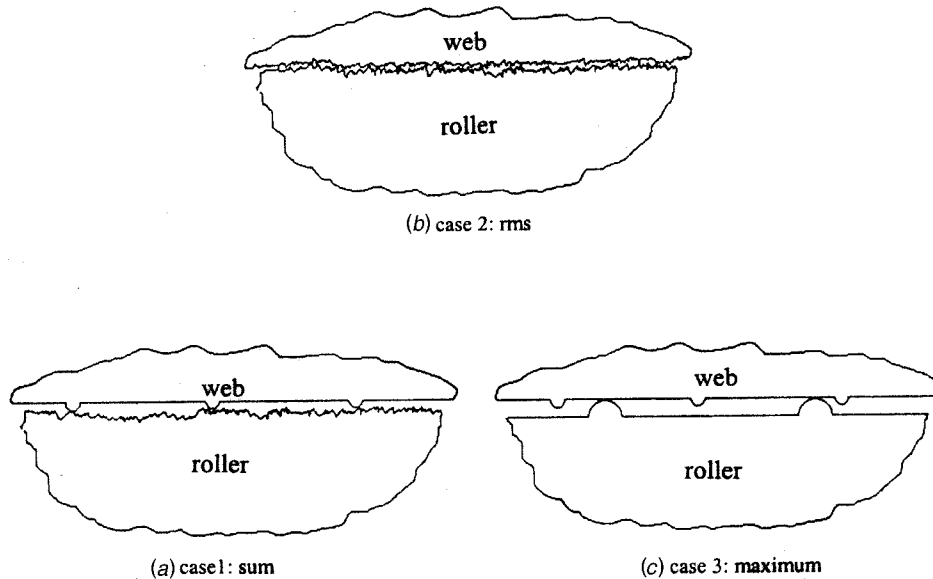


Fig. 9 Pictorial representation of how two rough surfaces might combine for various surface textures: (a) case 1: sum; (b) case 2: rms; and (c) case 3: maximum.

$$\alpha_c = \begin{cases} \alpha_r + \alpha_w & \text{sum-model} \\ \sqrt{\alpha_r^2 + \alpha_w^2} & \text{rms-model} \\ \max(\alpha_r, \alpha_w) & \text{max-model} \end{cases} \quad (9)$$

where the roller engagement height  $\alpha_r$  and the web engagement height  $\alpha_w$  are calculated using Eq. (8).

The optimized engagement height  ${}^m\alpha_c$  obtained from the mathematical model of the web/roller interface is compared to the engagement height model given in Eq. (9) in Table 5. The first column of this table is optimized  ${}^m\alpha_c$  values from Table 4. The second and third columns contain the web's engagement height  $\alpha_w$  calculated by Eq. (8) and the corresponding standard deviations. The fourth, fifth, and six columns contain the composite engagement height  $\alpha_c$  values (based on Eq. (9)), for the *sum-model*, the *rms-model*, and the *max-model*, respectively. The seventh and eighth columns contain sum and rms combinations of the web and roller  $R_z$  values. The last column of Table 5 lists the  $R_z/R_{pm}$  ratios of these surfaces. Comparison of the three  $\alpha_c$  values given in this table with the optimized engagement heights  ${}^m\alpha_c$  shows that for webs-1, 5, and 8 the *rms-model* is applicable, and for the other webs the *sum-model* is applicable. None of the webs requires the use of the *max-model*. The choice of the appropriate

model for each web is underlined. Asperity engagement based on the sum or rms of the  $R_z$  values correlates poorly with the optimized asperity engagement height values.

A close inspection of Table 5 shows that the appropriate choices are not arbitrary, but depend on the nature of the web and roller roughness. The nature of these contact heights can be better understood by studying Fig. 2, which shows the surface topography of the roller and the webs-1, 7, and 8 obtained with the optical surface profiler. Note that the surface of web-7 is representative of webs-2, 3, 4, and 6. Figure 2 shows that the asperities of web-1 and web-8 are more evenly distributed, compared to the few significant peaks that exist in web-7. Thus, it can be seen that the interfaces of webs-1 and -8 with the roller is similar to case-2, depicted in Fig. 9, and the interface of web-7 with the roller is similar to case-1.

The results presented in Table 5 indicate that in calculating the composite engagement height  $\alpha_c$  of a roller with a high  $R_z/R_{pm}$  ratio and a web:

- the sum-model is appropriate if the web surface has  $1.1 \leq R_z/R_{pm} < 1.4$

Table 5 Proposed engagement height model  $\alpha_c$  versus calculated optimal  ${}^m\alpha_c$

	${}^m\alpha_c$	$\alpha_w$		$\alpha_c$			$R_z$	$R_z$	$R_z/R_{pm}$
		mean	std	sum	rms	max	sum	rms	
roller	-	2.6 <sup>a</sup>	0.21 <sup>a</sup>	-	-	-	-	-	5.3
web 1	9.5	8.8	0.6	11.4	<u>9.1</u>	8.8	18.6	13.3	1.8
web 2	7.5	5.6	0.5	<u>8.3</u>	6.2	5.6	13.4	9.6	1.1
web 3	4.0	1.2	0.2	<u>3.8</u>	2.9	2.6	8.9	7.8	1.2
web 4	3.7	0.7	0.2	<u>3.3</u>	2.7	2.6	8.4	7.7	1.2
web 5	4.0	2.7	0.1	<u>5.3</u>	<u>3.8</u>	2.7	10.6	8.2	1.4
web 6	4.0	1.0	0.1	<u>3.6</u>	2.8	2.6	8.7	7.7	1.2
web 7	4.0	1.2	0.2	<u>3.8</u>	2.9	2.6	8.9	7.8	1.2
web 8	2.0	1.0	0.1	<u>3.6</u>	<u>2.8</u>	2.6	8.9	7.8	1.8

a. These are  $\alpha^t$  values.

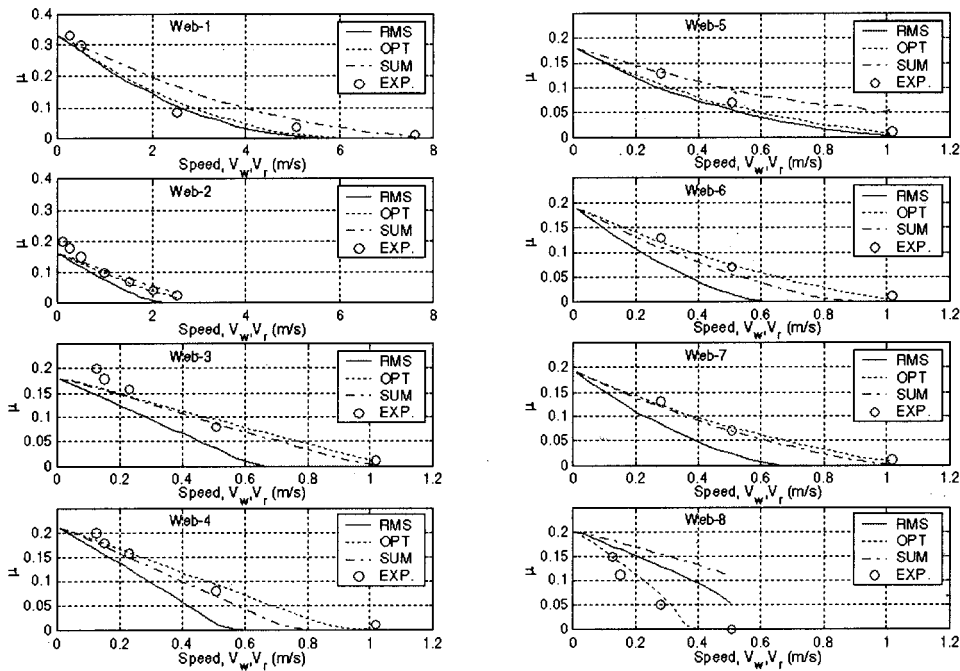


Fig. 10 Equivalent coefficient of friction: model prediction  ${}^m\mu_d$  versus actual measured  $\mu_d$  as a function of web speed

- the rms-model is appropriate if the web surface has  $1.4 \leq R_z/R_{pm} \leq 1.8$ .

While the limits for this methodology are somewhat arbitrary, observation of Table 5 shows that the procedure works well for all of the webs in this study.

### 5 The Effect of Engagement Height on Traction

Figure 10 shows the predicted equivalent coefficient of friction versus speed using each of the three estimates for the asperity engagement height. Results are shown for all eight webs. For webs 2, 3, 4, 6, and 7 the estimated  ${}^m\beta$  values are used, while for the other webs the  $\beta$  values obtained from compressibility measurements are used. The experimental data measured on the dynamic traction tester are also shown. It is again seen that in all cases the most appropriate asperity engagement model gives the

best agreement to the optimal predictions. Furthermore, in most cases, the agreement to the experimental data is very good. The only exception is the last case, web 8, where the model is shown to over predict the equivalent coefficient of friction.

The ability of the proposed model presented in this paper to accurately predict roller traction is shown in Fig. 11. For each of the eight webs of this study, the experimental speed at 50 percent traction loss is plotted against the predicted speed using the rms and sum asperity composite models. As can be seen, the predictions from the model are in good agreement with the experimental results. The data also shows clearly which roughness model is most appropriate for each web.

### Summary

An analytical model has been presented which predicts smooth roller traction as a function of speed. The model uses a simple two-parameter contact model, which expresses the relationship between the web-to-roller clearance and contact pressure. A heuristic model was developed to compute the asperity engagement height, based on  $R_{pm}$  and  $R_z$  measured with an optical surface profilometer. This model is general in that one or both surfaces may be rough and there is no restriction that their asperity height distributions need to be Gaussian. A method was also presented to estimate asperity compliance based on a stack compression test. For the web and roller combinations studied in this paper, asperity compliance had only a secondary effect on the equivalent coefficient of friction.

The traction loss over a roller was characterized experimentally for eight webs of different roughness characteristics. An error-minimization procedure was used to estimate the asperity engagement height and asperity compliance for the parabolic contact model from the traction experiments. These estimates compared favorably with asperity engagement height and asperity compliance based on optical surface profilometry and stack compression tests. These results confirm the viability and utility of these new test methods. The results of this work also confirmed that webs with high, distributed asperities perform better against traction loss.

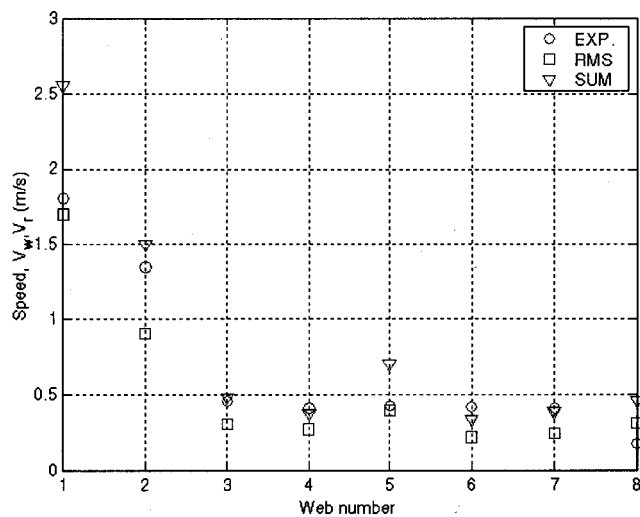


Fig. 11 Web speed at which the value of equivalent coefficient of friction  $\mu_d$  is reduced by 50 percent of its initial value  $\mu_0$

## Nomenclature

$c$  = web thickness  
 $D$  = bending stiffness of the web  
 $\varepsilon$  = error function  
 $E$  = Young's modulus of elasticity  
 $h$  = web-to-roller clearance  
 $k$  = shell stiffness of the web  
 $p$  = air pressure under the web  
 $P_{\text{atm}}$  = atmospheric pressure  
 $p_c$  = web-to-roller contact pressure  
 $F_c$  = web-to-roller contact force  
 $F_b$  = belt wrap force  
 $R$  = roller radius  
 $R_{pm}$  = surface roughness parameter, average of the five highest peaks in the sample, measured from the mean plane  
 $R_z$  = surface roughness parameter, difference between the average of the five highest peaks and the five lowest valleys in the sample, measured from the mean plane  
 $T$  = web tension per unit width  
 $V$  = transport velocity  
 $w$  = web displacement  
 $w_q$  = quiescent web displacement  
 $\alpha$  = asperity engagement height parameter  
 $\beta$  = asperity compliance parameter  
 ${}^m\alpha$  = optimized asperity engagement height parameter  
 ${}^m\beta$  = optimized asperity compliance parameter  
 $\delta$  = function used in defining web roller spacing  
 $\Delta T$  = roller tension difference on the dynamic traction tester  
 $\theta$  = roller wrap angle  
 $\lambda_a$  = molecular mean-free path of air  
 $\mu$  = kinetic coefficient of friction  
 $\mu_a$  = air viscosity  
 $x$  = longitudinal spatial coordinate  
 $\nu$  = Poisson's ratio  
 $\rho$  = mass density of the web

## Subscripts

$a$  = average tension

$c$  = combined web and roller  
 $d$  = dynamic traction tester  
 $i, e$  = roller entrance, exit  
 $m$  = model  
 $o$  = low speed, 0.005 m/s  
 $r$  = roller  
 $w$  = web  
 $s$  = single surface

## References

- [1] Daly, D. A., 1965, "Factors Controlling Traction Between Webs and Their Carrying Rolls," *Tappi J.*, **48**, No. 9, pp. 88–90.
- [2] Forrest, A. W., Jr., and Anderson, V. L., 1997, "Film Surface Considerations for Enhancing Winding of Thin Films," *Proceedings of the Fourth International Conference on Web Handling*, Oklahoma State University.
- [3] Knox, K. L., and Sweeney, T. L., 1971, "Fluid Effects Associated with Web Handling," *Ind. Eng. Chem. Process Des. Dev.*, **10**, No. 2, pp. 201–205.
- [4] Eshel, A., and Elrod, H. G., Jr., 1965, "The Theory of the Infinitely Wide, Perfectly Flexible, Self-Acting Foil Bearing," *Journal of Basic Engineering*, *Trans. of the ASME*, March 1959, pp. 94–100.
- [5] Ducotey, K. S., and Good, J. K., 1995, "The Importance of Traction in Web Handling," *ASME J. Tribol.*, **117**, pp. 679–684.
- [6] Müftü, S., and Altan, M. C., 2000, "Mechanics of a Porous Web Moving Over a Cylindrical Guide," *ASME J. Tribol.*, **122**, pp. 418–426.
- [7] Greenwood, J. A., and Williamson, J. B. P., 1966, "Contact of Nominally Flat Rough Surfaces," *Proc. R. Soc. London, Ser. A*, **295**, pp. 300–319.
- [8] Kikuchi, N., and Oden, J. T., 1988, *Contact Problems in Elasticity: A Study of Variational Inequalities and Finite Element Methods*, SIAM, Philadelphia.
- [9] Lacey, C., and Talke, F. E., 1992, "Measurement and Simulation of Partial Contact at the Head/Tape Interface," *ASME J. Tribol.*, **114**, pp. 646–652.
- [10] Wu, Y., and Talke, F., 1996, "The Effect of Surface Roughness on the Head-Tape Interface," *ASME J. Tribol.*, **118**, No. 2, pp. 376–381.
- [11] Burgdorfer, A., 1959, "The Influence of the Molecular Mean Free Path on the Performance of Hydrodynamic Gas Lubricated Bearings," *Journal of Basic Engineering*, *Trans. of the ASME*, December 1965, pp. 831–836.
- [12] Müftü, S., and Cole, K. A., 1999, "The Fluid/Structure Interaction in Supporting a Thin Flexible Cylindrical Web with an Air Cushion," *J. Fluids Struct.*, **13**, pp. 681–708.
- [13] Müftü, S., and Benson, R. C., 1995, "Modeling the Transport of Paper Webs Including the Paper Permeability Effects," *Advances in Information Storage and Processing Systems, ASME International Mech. Eng. Congress and Exposition, San Francisco, CA, ISPS-Vol. 1*, pp. 247–258.
- [14] Gross, W. A., 1980, *Fluid Film Lubrication*, John Wiley & Sons, New York.
- [15] ASTM Standard G143-96, 1996, "Standard Test Method for Measurement of Web/Roller Friction Characteristics," *Annual Book of ASTM Standards*.
- [16] Bhushan, B., 1996, *Tribology and Mechanics of Magnetic Storage Devices*, Springer-Verlag Inc., New York.